

Accelerated oxygen evolution kinetics on Ir-doped $SrTiO_3$ perovskite by NH_3 plasma treatment

Li-Li Deng(邓丽丽), Xiao-Ping Ma(马晓萍), Man-Ting Lu(卢曼婷), Yi He(何弈), Rong-Lei Fan(范荣磊), and Yu Xin(辛煜)

Citation: Chin. Phys. B, 2022, 31 (**11**): 118201. DOI: 10.1088/1674-1056/ac70b1

What follows is a list of articles you may be interested in

Near-infrared photocatalysis based on upconversion nanomaterials

Xingyuan Guo(郭星原), Zhe Wang(王哲), Shengyan Yin(尹升燕), and Weiping Qin(秦伟平)

Chin. Phys. B, 2022, 31 (**10**): 108201. DOI: 10.1088/1674-1056/ac7556

Lithium ion batteries cathode material: V_2O_5

Baohe Yuan(袁保合), Xiang Yuan(袁祥), Binger Zhang(张冰儿), Zheng An(安政), Shijun Luo(罗世钧), and Lulu Chen(陈露露)

Chin. Phys. B, 2022, 31 (**3**): 038203. DOI: 10.1088/1674-1056/ac21be

Improved electrochemical performances of high voltage $LiCoO_2$ with tungsten doping

Jie-Nan Zhang(张杰男), Qing-Hao Li(李庆浩), Quan Li(李泉), Xi-Qian Yu(禹习谦), Hong Li(李泓)

Chin. Phys. B, 2018, 27 (**8**): 088202. DOI: 10.1088/1674-1056/27/8/088202

Understanding oxygen reactions in aprotic Li-O_2 batteries

Shunchao Ma(马顺超), Yelong Zhang(张业龙), Qinghua Cui(崔清华), Jing Zhao(赵婧), Zhangquan Peng(彭章泉)

Chin. Phys. B, 2016, 25 (**1**): 018204. DOI: 10.1088/1674-1056/25/1/018204

Surface morphology and electrochemical characterization of electrodeposited Ni–Mo nanocomposites as cathodes for hydrogen evolution

Elhachmi Guettaf Temam, Hachemi Ben Temam, Said Benramache

Chin. Phys. B, 2015, 24 (**10**): 108202. DOI: 10.1088/1674-1056/24/10/108202

Accelerated oxygen evolution kinetics on Ir-doped $SrTiO_3$ perovskite by NH_3 plasma treatment

Li-Li Deng(邓丽丽), Xiao-Ping Ma(马晓萍), Man-Ting Lu(卢曼婷), Yi He(何弈), Rong-Lei Fan(范荣磊)†, and Yu Xin(辛煜)‡

School of Physical Science and Technology, Jiangsu Key Laboratory of Thin Films, Soochow University, Suzhou 215006, *China*

(Received 7 January 2022; revised manuscript received 30 April 2022; accepted manuscript online 18 May 2022)

Exploring low-cost and high-performance catalysts for oxygen evolution reaction (OER) remains to be a great challenge. Iridium-based perovskite oxide has large potential in OER because of its intrinsic activity and outstanding physicochemical properties. In this study, iridium-doped strontium titanate (Ir-STO) solution is brushed on a Ti sheet by the traditional method to obtain the Ir-STO/Ti electrodes after being calcined at a high temperature. The microstructure and electrocatalysis properties of the Ir-STO are further modified by a facile and scalable NH_3-plasma strategy. In addition to the doping of Ir, the NH_3 plasma treatment further results in N-doping into Ir-STO, which enriches active species and causes oxygen vacancies near doped sites. The resulting N, Ir-STO/Ti electrode reveals excellent acidic OER activity with the lowest overpotential of 390 mV at 10 mA/cm^2 and the smallest Tafel slope of 140 mV/dec after 10-min plasma treatment. Therefore, the great potential of activated N, Ir-STO/Ti is regarded as a catalyst for the OER, and thus making a new opportunity for developing other perovskite catalysts via NH_3 plasma treatment.

Keywords: electrocatalysts, NH_3 plasma, oxygen vacancies, N doping

PACS: 82.45.Hk, 82.45.Jn, 52.77.Dq, 74.62.Dh **DOI:** 10.1088/1674-1056/ac70b1

1. Introduction

Electrochemical splitting of water to produce hydrogen driven by renewable feedstocks (generated from wind or solar, *etc*.) is considered to be a promising approach to mass production of hydrogen in the future.[1–3] However, the anodic semi-reaction-oxygen evolution reaction (OER) process of water splitting requires an inevitable dynamic overpotential, resulting in high energy consumption.[4,5] Noble metal oxides such as IrO_2 and RuO_2 are known as the most effective OER catalysts, but their low reserves and high cost greatly limit the large-scale commercial applications.[6–8] Therefore, it is urgent to develop highly active electrocatalysts with low noble metal content.

A great deal of research has been done on transition metal-based materials.[9] Among them, perovskite oxides have attracted considerable attention because of their low price, good stability and adjustable physicochemical properties.[10–12] The general formula for perovskite is ABO_3, where transition metal B plays a key role in the catalytic process. Seitz *et al*.[13] demonstrated the role of B site in perovskite by the epitaxial growth of $SrIrO_3$ films on the surface of $SrTiO_3$ catalyst. Metal-ions doping is recognized as an efficient strategy to improve intrinsic electronic conductivity and modulate electrocatalytic activity.[14] Actually, on the premise of ensuring the structural stability of perovskite, introducing metal ions with different charges or sizes into the perovskite crystal lattice can make the lattice strain, thus adjusting the oxidation state.[15] Liang *et al*.[16] synthesized solid solution perovskite Ir-STO by polymerization complex method. Ir doping activated the inert STO matrix to generate Ti sites with catalytic activity. They found the synergistic effect of Ir and Ti to enhance the oxygen adsorption on the surface in the case of reduced iridium consumption.

Notably, when metal cations are doped into perovskite, oxygen vacancies will be induced in perovskite crystals due to the electroneutrality principle.[17] Mefford *et al*.[18] and She et al.[19] have confirmed the change of the oxygen vacancy concentration in $La_{1-x}Sr_xCoO_{3-\delta}$ and $La_{1-x}Sr_xFeO_{3-\delta}$ perovskites with substitution of La^{3+} by Sr^{2+}, respectively. Other studies showed that oxygen vacancies in metal oxides can improve the catalytic activity of OER oxides by reducing the adsorption energy of water.[20,21] Plasma treatment can effectively carve oxides, selectively remove oxygen on the surface, and produce oxygen vacancies.[22] Under the bombardment of high-energy ions (Ar^+, N^{2+}, H_2O^+), oxygen vacancies can be created on metal oxide surfaces. Lu *et al*.[23] replaced the La site with Sr in $LaCoO_3$, and then treated the sample with Ar plasma, resulting in the increase of the oxygen vacancies and a large number of active sites with high OER activity and stability.

Recent studies have shown that the performance of perovskite-based catalysts can be improved by introducing non-metallic elements (such as P, N, S, *etc*.) into the perovskite lattice to change the surface properties and elec-

†Corresponding author. E-mail: rlfan@suda.edu.cn
‡Corresponding author. E-mail: yuxin@suda.edu.cn

© 2022 Chinese Physical Society and IOP Publishing Ltd

tron/phase structure of perovskite.[24–26] Owing to different properties of nitrogen and oxygen (such as polarizability, electronegativity and charge), the introduction of N into perovskite oxide can change the physical and chemical properties.[26] Specifically, since N is less electronegative than O, N-doping can reduce the bandgap, thus improving electron transport in perovskite oxides.[27,28] The N partially replaces the O in perovskite oxides, forming perovskite with abundant oxygen vacancies and high oxidation states of B-site metal cations.[29] Zhang *et al*.[30] doped $LaNiO_3$ with N, which significantly increases the Ni^{3+} content and the surface oxygen vacancies and promotes the anodic oxygen evolution reaction. In our experiment, we have found that the concentration of oxygen vacancies can be optimized by N, Ir doping into the STO matrix.

In this paper, in order to improve OER electrocatalytic performance, two strategies are employed for $SrTiO_3$ perovskites to generate oxygen vacancies. First, we partially replace Ti with Ir to change the electrocatalytic performance of $SrTiO_3$. Then, N doping into the Ir-STO coatings by using NH_3 plasma treatment to produce oxygen vacancies. The Ir-STO coatings will be synthesized by high-temperature thermal decomposition on titanium sheets. The atomic ratio of Ir to Ti is 1:2, significantly reducing the amount of iridium used compared with the industrial proportion of 70% such as in the IrO_2/RuO_2 system.[31] And then, capacitively coupled NH_3 plasma is used to treat the above samples and thus to adjust oxygen vacancies in the bulk. Herein, a 13.56-MHz-driven capacitively coupled NH_3 plasma with input power of 300 W is chosen with the different treatment times for the Ir-STO/Ti samples. The samples are characterized by using field emission-scanning electron microscopy (FE-SEM), x-ray diffractometer (XRD), x-ray photoelectron spectroscopy (XPS), and electrochemical workstation.

2. Experiment

2.1. Synthesis of Ir-STO/Ti

A Ti sheet (0.5-mm thick) with an exposed surface area of 1 cm×1 cm was used. It was sandblasted, ultrasonically cleaned for 10 min in a 15-vol% Na_2CO_3 solution, and then etched for 30 min in oxalic acid (15 vol%). $Sr(NO_3)_2$, $C_{16}H_{36}O_4Ti$, and $H_2IrCl_6{\cdot}6H_2O$ were dissolved in a mixture of glycol and citric acid (the ratio of glycol to citric acid was 9:1) to form the precursor solution, sequentially. The Ti sheet was brushed with the precursor solution and then annealed in a muffle furnace at 300 °C for 10 min. The above process was repeated three times, and finally, the samples were annealed at 600 °C for 4 h to fabricate Ir-STO/Ti electrodes.

The fabricated Ir-STO/Ti electrodes were then treated by capacitively coupled NH_3 plasma to dope N atoms in the Ir-STO/Ti. The annealed Ir-STO/Ti was transferred into the capacitively coupled plasma (CCP) chamber with the discharge power of 300 W and the NH_3 flow rate of 80 sccm, and the samples were placed about 1 cm away from the lower plate to conduct double-sided treatment. The working pressure was set to be 5 Pa and the bias voltage to be 452 V nominally. In order to avoid large damage to Ir-STO/Ti due to plasma-induced degradation (PID), the treatment time of Ir-STO/Ti was controlled within 20 min. For controlling the nitridation degree, the treatment was performed for different durations of 5 min, 10 min, 15 min, and 20 min, and the corresponding samples were denoted as N, Ir-STO /Ti-5 min, N, Ir-STO/Ti-10 min, N, Ir-STO/Ti-15 min, and N, Ir-STO/Ti-20 min, respectively.

2.2. Characterizations of structure

The crystal structure of the prepared samples were analyzed by using an XRD with bruker D8 advance diffractometer at a scanning range of 20°–80°. The surface morphology of the prepared Ir-STO/Ti and N, Ir-STO/Ti electrodes were characterized via FESEM with a Regulus Su8100 microscope. The chemical composition information of the samples was tested by XPS with a Thermo ESCALAB250XI spectrometer. The information about oxygen vacancies in Ir-STO/Ti and N, Ir-STO/Ti coatings were measured by electron spin resonance spectrometer (EPR, Model JES-X320, Japan).

2.3. Electrochemical measurements

Electrochemical tests were performed on a standard three-electrode system of electrochemical workstation. A three-electrode system consists of a working electrode with electrocatalyst of Ir-STO/Ti and N, Ir-STO/Ti, a platinum plate as the counter electrode and a saturated calomel electrode (SCE) as a reference electrode. From the following formula calculated are all potentials of the reversible hydrogen electrode (RHE) in this paper:

$$E(\textit{versus}\ \text{RHE}) = E(\textit{versus}\ \text{SCE}) + 0.2412\ \text{V} + 0.059\text{V} \times \text{pH}. \quad (1)$$

The linear scanning voltammetry (LSV) polarization curves were measured in a 0.5-M H_2SO_4 solution from 1.0 V to 1.8 V (*versus* RHE) in potential steps of 5 mV/s. The cyclic voltammogram (CV) curves were made between 0.1 V and 1.5 V (*versus* RHE) at a scan rate of 50 mV/s through experiments in 0.5-M H_2SO_4 solution. Electrochemical impedance spectroscopy (EIS) was used at a voltage of 1.7 V (*versus* RHE) and AC sinusoidal signal amplitude of 5.0 mV, and in a frequency range of 100 kHz–0.1 Hz. ZSimpDemo software is used to fit EIS data in the corresponding equivalent circuit.

3. Results and discussion

Interaction of plasma with surface of materials plays a crucial role in the modification of semiconductor

fabrication.[32] However, the heavy elements for the Ir-STO/Ti may not be easily etched by NH_3 plasma treatment even under the ion bombardment due to ineffective momentum transfer in between. The SEM results (not shown here) demonstrate that the morphologies of the samples do not change significantly, indicating little effect of the plasma treatment on the morphology of perovskites.[23,33] Under the action of ion bombardment, the elements with small mass O in the Ir-STO coating surface can be easily etched under the bombardment of high energy ions of N_2^+, NH^+, *etc*. Some of the neutral groups such as NH_x, N in the plasma will diffuse onto the surface and fill in these vacancies with great probability, although they are also bombarded by ions. Therefore, the displacement reaction will occur in between the active species such as NH_x, N, *etc*. in the NH_3 plasma[34] and lattice O atom in the Ir-STO coatings. This is an important reason for N atoms to dope into the perovskite matrix under the plasma action, confirmed by the XRD and XPS characterization.

The XRD results, depicted in Fig. 1(a), confirm that the STO/Ti sample and Ir-STO/Ti sample each present a perovskite-type phase. In comparison, no evident new peaks are observed in the XRD patterns but the diffraction peak ($SrTiO_3$) gradually shifted toward small diffraction angles due to the doping Ir into STO/Ti as indicated in the inset of Fig. 1(a). Considering that the measurement error of this instrument is 0.01°, we can confirm that the slight shift ($0.09° \pm 0.01°$, 2θ) originates from a high ionic radius iridium dopant into STO/Ti ($Ir^{4+} = 62.5$ pm, $Ti^{4+} = 60.5$ pm).[16] Figure 1(b) shows the crystal structure of samples after NH_3 plasma treatment, the bulk crystal structure does not change much in comparison with Ir-STO/Ti matrix. From the detailed observation of XRD patterns, it is found that the typical $SrTiO_3$ (110) diffraction peak of N, Ir-STO/Ti shown in Figs. 1(c)–1(d), shifts toward high diffraction angles in comparison with pristine Ir-STO/Ti. The shifting of 2θ value can be attributed to two main factors. On the one hand, at the beginning of NH_3 plasma treatment, numerous energetic particles rapidly attack and react with surface lattice oxygen to form oxygen vacancies.[35] The charge neutrality after the generation of oxygen vacancies is compensated for by the reduction of Ti^{4+} (0.605 Å) into Ti^{3+} (0.670 Å).[36] On the other hand, the N atoms can easily occupy the oxygen vacancies, thus replacing the O atom positions and dope into substitutional sites, resulting in the modification of the electronic states.[37] As mentioned above, it seems that N and Ir doping may adjust the lattice parameter of STO/Ti.

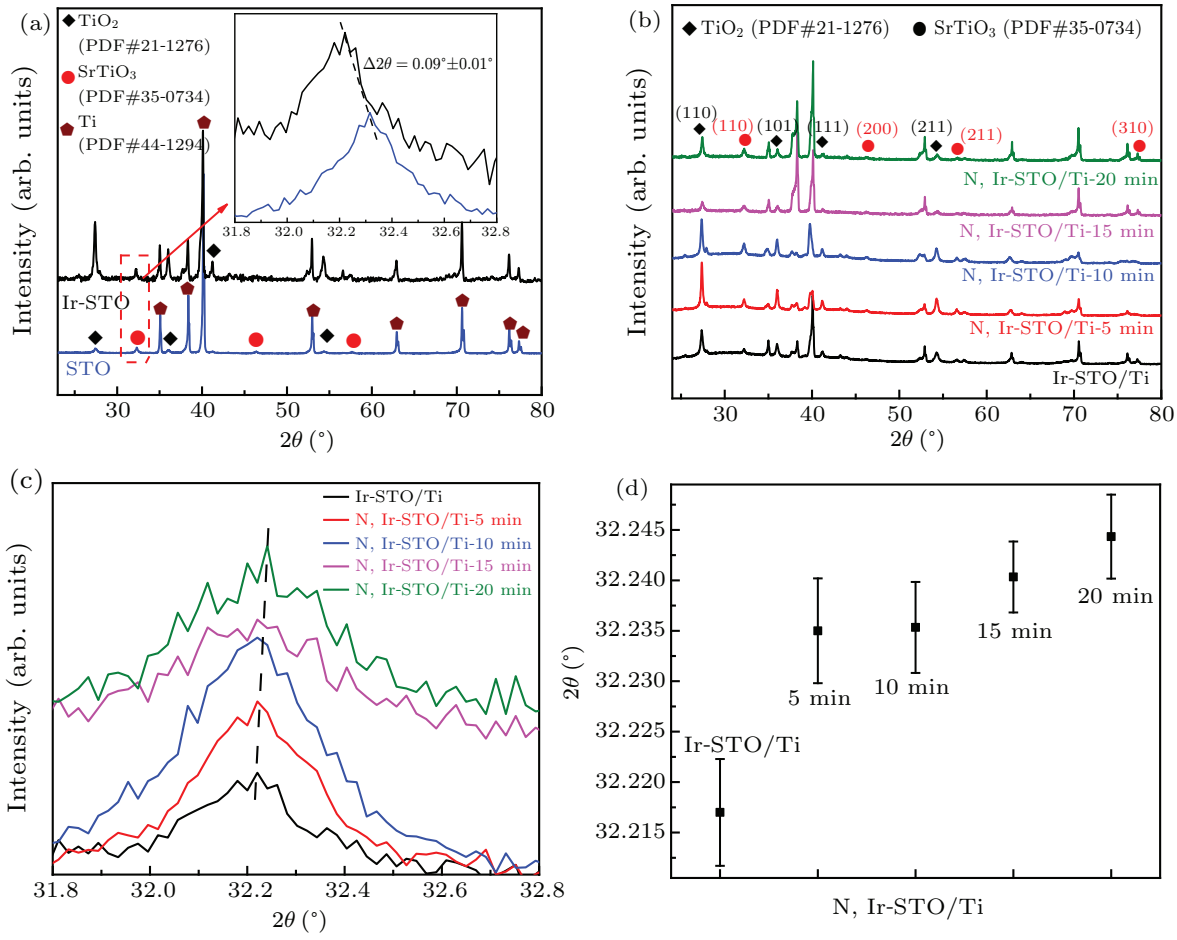


Fig. 1. XRD patterns of (a) Ir-STO/Ti and STO/Ti, with inset showing magnified part of patterns between 31.8°–32.8°; (b) XRD patterns of Ir-STO/Ti and N, Ir-STO/Ti treated by NH_3 plasma for 5 min, 10 min, 15 min, 20 min, respectively; (c) magnified XRD patterns with 2θ between 31.8°–32.8°; (d) error bar of typical $SrTiO_3$ (110) diffraction peak.

The most direct evidence to determine whether N doping exists in Ir-STO/Ti sample comes from XPS analysis. The XPS measurement spectra indicate that besides the presence of Ir, Ti, Sr, and O, the information from N of Ir-STO/Ti samples treated by the NH_3 plasma also appears as shown in Fig. 2(a). It can be seen from Fig. 2(b) that N 1s chemical state changes greatly with the increase of NH_3 plasma treatment time. The N 1s XPS spectrum as shown in the figure can be well fitted to three characteristic peaks: oxynitride (Ir/Ti–O–N) species (399.8 eV), Ir–N bond (397.7 eV), and Ti–N bond (396.2 eV), respectively.[38–40] Various peaks of N 1s binding energy between 395.8 eV and 397.8 eV can be found elsewhere,[41] which are generally considered as being from other nitrogen source. These findings suggest that N may be introduced into Ir-STO/Ti lattice as the alternative dopant by NH_3 plasma treatment. Compared with Ir-STO/Ti, the peaks of Ir–N and Ti–N for the N, Ir-STO/Ti samples increase gradually with the increase of plasma treatment time, indicating an effective N-doping in the Ir-STO/Ti matrix.

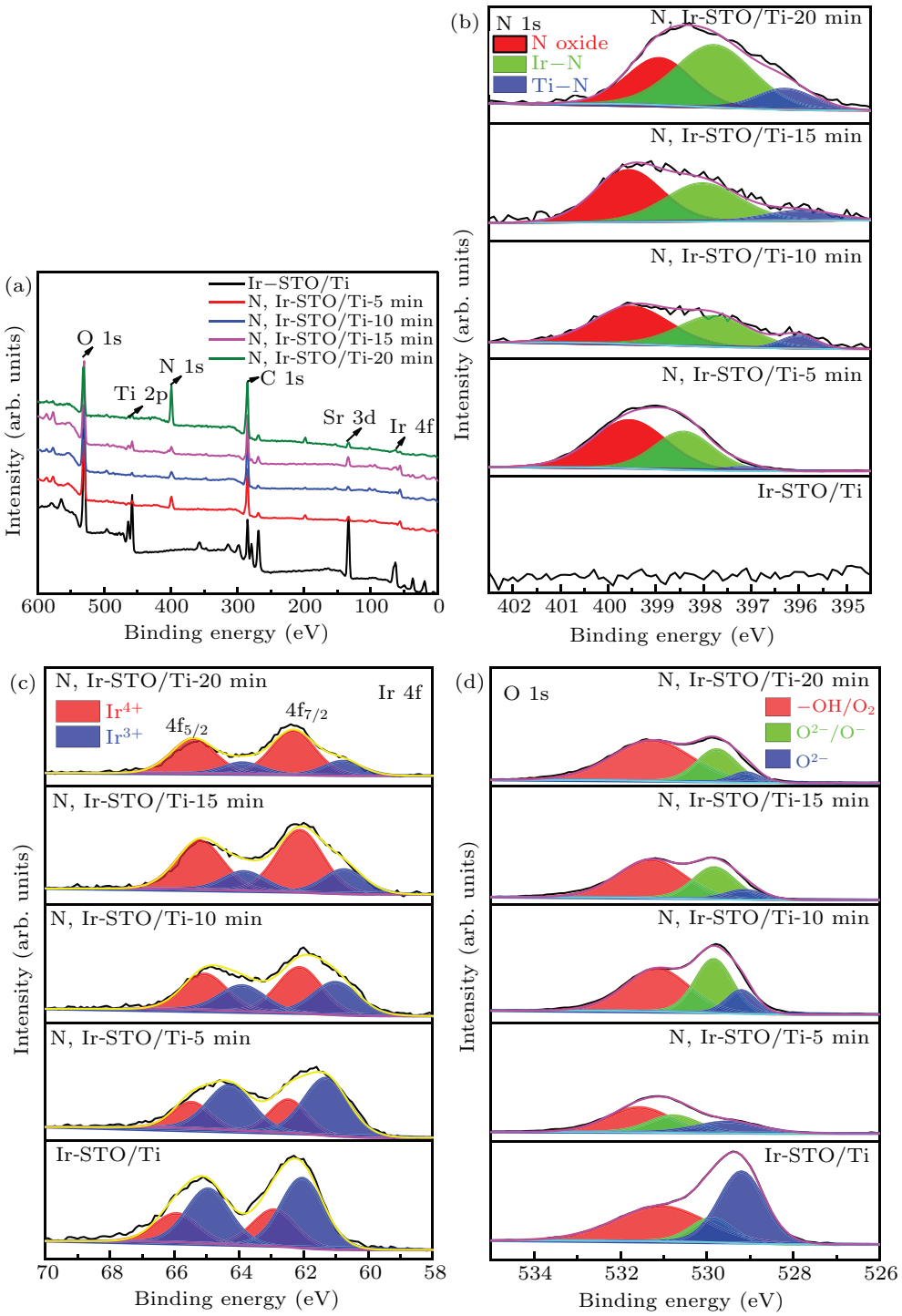


Fig. 2. XPS spectra of Ir-STO/Ti and N, Ir-STO/Ti with different NH_3 plasma treatment times: (a) survey spectra, (b) high resolution spectra of N 1s, (c) Ir 4f, and (d) O 1s.

Table 1. XPS data fitting results of different Ir and O species of Ir-STO/Ti and N, Ir-STO/Ti with different NH_3 plasma treatment times.

Peak	Assignment	Proportion of specie				
			N, Ir-STO/Ti			
		Ir-STO/Ti	5 min	10 min	15 min	20 min
Ir 4f	Ir^{3+}/Ir	0.82	0.28	0.25	0.24	0.22
	Ir^{4+}/Ir	0.18	0.72	0.75	0.76	0.78
	Ir	0.11	0.09	0.08	0.05	0.02
O 1s	–OH/O_2	0.39	0.50	0.43	0.50	0.58
	O_2^{2-}/O	0.18	0.27	0.42	0.39	0.33
	O^{2-}	0.43	0.23	0.16	0.11	0.09

Owing to charge balancing in the N, Ir-STO/Ti, the incorporation of Ir and N atoms into the STO matrix may cause the valence state of the iridiumon the B-site to change. Figure 2(c) shows that the Ir 4f spectra of the samples reveal two doublets corresponding to the spin–orbit components Ir $4f_{7/2}$ and Ir $4f_{5/2}$, respectively. The doublets are divided into Ir^{3+} $4f_{7/2}$ (61.40 eV), Ir^{4+} $4f_{7/2}$ (63.01 eV), Ir^{3+} $4f_{5/2}$ (64.30 eV), and Ir^{4+} $4f_{5/2}$ (66.01 eV).[42,43] Therefore, by integrating the peak area, the relative values of content of these Ir species are calculated as shown in Table 1. The Ir content decreases possibly due to its relatively high sputtering yield. The Ir^{4+} content of the samples treated by NH_3 plasma increases significantly. This may be due to the charge compensation caused by N and Ir co-doping.[29] Interestingly, the Ir^{4+} state may activate the inert STO matrix, generate efficient Ti catalytic sites, thus improving the performance of the catalyst.[16]

The incorporation of Ir and N into the STO matrix causes a slight change both in the lattice parameters as mentioned before and in the chemical state of O changes. The O 1s spectra are collected from the Ir-STO/Ti and N, Ir-STO/Ti samples as shown in Fig. 2(d). Typical peaks at 529.20 eV, 529.9 eV, and 531.2 eV correspond to the lattice oxygen (O^{2-}), highly oxidative oxygen species (O^{2-}/O^-), and hydroxyl groups or surface-adsorbed oxygen species (–OH/O_2), including –OH, O^-, and O_2^{2-}, respectively.[40,44] In Table 1 listed are the relative values of content of each oxygen-related species for these N, Ir-STO/Ti coatings, which are obtained from the area ratio of corresponding speak. It should be pointed out that the relative value of content of O^{2-}/O^- species is closely related to surface oxygen vacancies.[45] It can be seen that the N, Ir-STO/Ti coating treated with plasma for 10 min shows the highest content of O^{2-}/O^- (0.42) in all the samples, which means that the quantity of oxygen vacancies is the highest. Note that the increasing of NH_3 plasma treatment time leads the O^{2-}/O^- content in N, Ir-STO/Ti coatings to decrease slightly. It may be due to the fact that excessive N atoms occupy oxygen vacancies, thereby replacing O sites and doping into the substitution sites.[46] Additionally, the increased –OH/O_2 content of the N, Ir-STO/Ti samples compared with that of the Ir-STO/Ti indicates the enhanced hydrophilicity of the catalyst, which can increase the adsorption of oxygen species on the catalyst surface, thus improving the catalytic activities.[47]

The changes of oxygen vacancies for the N, Ir-STO/Ti coatings are further probed by the low-temperature electron paramagnetic resonance (EPR) spectrum. As shown in Fig. 3, Ir-STO/Ti and N, Ir-STO/Ti coatings each present a response at a g-value of 2.003, indicating the existence of isolated oxygen vacancies. It can also be seen from Fig. 3 that the peak value of EPR increases gradually when the plasma treatment time is less than 10 min and decreases gradually when the plasma treatment time is more than 10 min. For the plasma treatment time of 10 min, the peak value of EPR is the strongest, indicating the highest oxygen vacancy content in N, Ir-STO/Ti coating. The results from EPR are consistent with the XPS analysis ones obtained before. The ions from the bulk plasma will bombard the sample surface, oxygen bonded to either Ti or Ir on the surface of matrix will be sputtered or etched by ions or the other active species such as NH_x and N. The presence of N dopant facilitates the formation of oxygen vacancies. As a result, suitable plasma treatment of 10 min can improve the vacancy density. With excessive plasma treatment, more oxygen vacancies including oxygen vacancies caused by Ir doping will be replaced by N atoms. That is to say, the incorporation of both N and Ir into the STO matrix may modulate the oxygen vacancies in the bulk.[48]

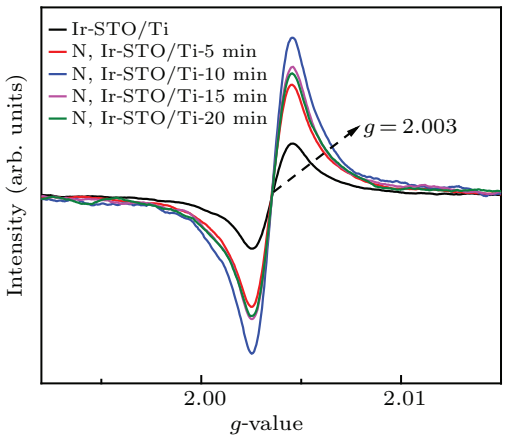


Fig. 3. EPR spectra of Ir-STO/Ti and N, Ir-STO/Ti with different NH_3 plasma treatment times.

The LSV tests are conducted to measure some parameters

of Ir-STO/Ti and N, Ir-STO/Ti electrodes at 5-mV/s scanning rate in 0.5-M H_2SO_4 solution. As shown in Fig. 4(a), the OER catalytic activity of Ir-STO/Ti is remarkable with an overpotential of 410 mV at a current density of 10 mA/cm^2, while the OER activity of STO/Ti is negligible. This result indicates that Ir doping enhances the OER activity of STO/Ti, which is consistent with the result from other research.[16] Figure 4(b) shows the LSV curves of Ir-STO/Ti treated by NH_3 plasma for different treatment times. It is found that the N, Ir-STO/Ti-10-min catalyst exhibits the best activity with the smallest overpotential of 390 mV at a current density of 10 mA/cm^2. Basically, the N, Ir-STO/Ti coatings show better activity than Ir-STO/Ti except the one with 20 min. Owing to the saturation of oxygen vacancy and the decrease of Ir content, the electrocatalytic activity of N, Ir-STO/Ti-20-min electrode is lower than that of Ir-STO/Ti. Among them, the lowest Tafel slope of N, Ir-STO/Ti-10 min (140 mV/dec) is also found as shown in Fig. 4(c).

Figure 4(d) shows the voltammetry curves of various samples recorded at a scanning rate of 50 mV/s in a 0.5-M H_2SO_4 solution. The pair of peaks at 1 V–1.2 V (*versus* RHE) are attributed to the surface redox transition of Ir(III)/Ir(IV), which is a pair of typical redox peaks in the electrochemical process of Ir-based electrocatalysts.[49,50] Within this 0.4 V–1.44 V potential range, hydrogen evolution reaction or OER will not occur on the electrode surface. Under this condition, the current belongs to the electric double layer charging current.[51,52] Integrating the CV curve in this potential range can obtain the voltammetric charge capacity (q^*), which represents the number of protons exchanged by the electrode with the solution.[53] The q^* is proportional to the electrochemically active surface area of the oxide electrode (EASA),[54] and can reflect the number of electrochemically active centers on the surface of the electrode. Figure 4(e) shows the highest EASA of about 200 mC/cm^2 for the N, Ir-STO/Ti-10 min sample. Meanwhile, the electrochemical double-layer capacitance (C_{dl}) for the sample in Fig. 4(f) also shows the highest value of 6.18 mF/cm^2.

Figure 5 shows the impedance spectra of the Ir-STO/Ti and N, Ir-STO/Ti samples in a 0.5-M H_2SO_4 solution. The resistance of the H_2SO_4 solution is characterized by R_s, which is connected in series with the coating system unit.[55] The R_{ct} is the resistance of charge transfer on the electrode solution interface, and its value reflects the electrocatalytic activity of OER.[56] The Q_{dl} value represents the number of active points on the inner surface of the coating.[57,58] The fitted EIS data for all the electrical parameters are listed in Table 2. The Q_{dl} value of the sample treated by NH_3 plasma for 10 min is significantly higher than those of other samples, indicating that the NH_3 plasma treatment for 10 min can maximize the number of active points on the coating surface. Moreover, the R_{ct} (11.10 Ω/cm^2) value of NH_3 plasma-treated samples for 10 min is the smallest, implying a better conductivity. This test result is consistent with the polarization measurement mentioned above.

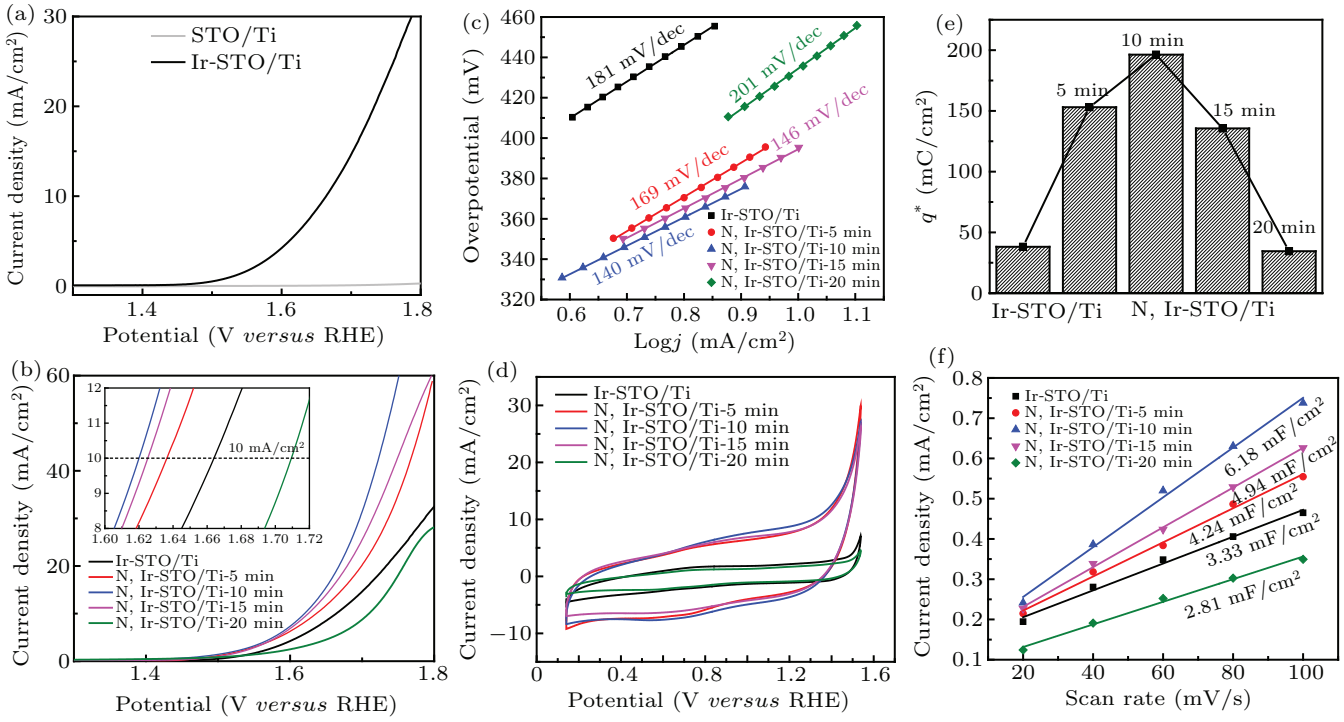


Fig. 4. (a) Polarization curves of pristine STO/Ti and the Ir-STO/Ti. (b) Polarization curves of Ir-STO/Ti and N, Ir-STO/Ti, with inset showing chronopotentiometry test at 10 mA/cm^2. (c) Corresponding Tafel plots. (d) CV curves of Ir-STO/Ti and N, Ir-STO/Ti. (e) Voltammetric charges obtained by integrating the curves. (f) Value of C_{dl} for the Ir-STO/Ti and N, Ir-STO/Ti with different NH_3 plasma treatment times.

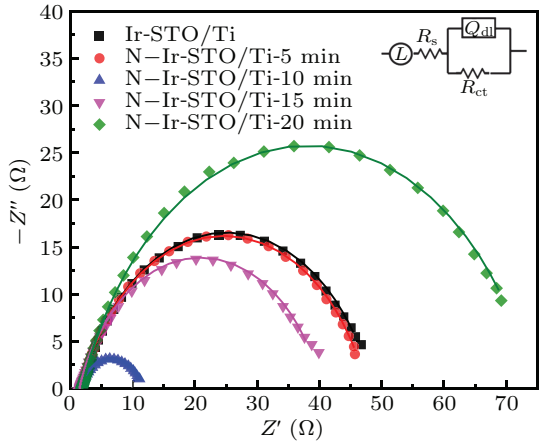


Fig. 5. Nyquist plots of N, Ir-STO/Ti prepared by different times, with inset showing equivalent circuit model.

Table 2. Fitting EIS parameters of Ir-STO/Ti and N, Ir-STO/Ti samples.

N, Ir-STO/Ti	R_s (Ω/cm^2)	R_{ct} (Ω/cm^2)	Q_{dl} (Ω^{-1}·cm^{-2}·S^n)
Ir-STO/Ti	1.49	46.7	0.0617
5 min	1.76	45.71	0.0650
10 min	1.54	11.1	0.1851
15 min	1.71	40.12	0.0652
20 min	1.61	69.21	0.0509

For 13.56-MHz-driven capacitively coupled NH_3 plasma, active species such as NH_2, H, and N can be observed by optical emission spectra.[59] As these species transport into the material surface, interaction in between will occur. Among them, extreme reducible H atom causes the metal oxides to reduce to metal by hydrogen reacting with oxygen atoms on the surface. For STO, the large bond energies of Sr–O and Ti–O (426.3 kJ/mol, 666.5 kJ/mol)[60] become a little bit difficult to reduce H atoms. It is noteworthy that the treated samples are placed on the powered electrode surface, the self-bias on the sheath approaches to −360 V as 300-W radio frequency power is applied. For the treatment condition, discharge pressure is set to be 5.0 Pa, that is, ion acceleration during transportation through sheath will endure collision with neutral particles less than 4 times averagely due to ion mean free path of 1.2 mm and the calculated sheath width of about 3.7 mm. Ion energy to the STO surface on the powered electrode is enough to cause Ti–O or Sr–O bonds to break. Thus, in the combination of ion bombardment assistance, the reduction of H atom on the STO surface becomes relatively easy. As O atom is devoured by the H atom, the left sites will be occupied by N-containing species with a significant probability. A shift of STO/Ti lattice (110) diffraction peak to a lower angle in XRD and the appearance of N element and its change of chemical state in XPS have confirmed the binding of N into Ir-STO/Ti matrix. Additionally, from the diffraction angle in the opposite direction due to N and Ir doping in Fig. 1, it can be inferred that the two kinds of elements can modulate the lattice parameters of N, Ir-STO/Ti. From Fig. 4, N and Ir doping may optimize the bulk oxygen vacancies with a maximal vacancy concentration at 10-min NH_3 plasma treatment. Therefore, the best electrocatalytic performance of N, Ir-STO/Ti coatings is observed with NH_3 plasma treatment time increasing up to 10 min.

4. Conclusions

In summary, we have successfully created more O vacancies in $SrTiO_3$ perovskite by Ir doping and NH_3 plasma treatment. By combining two techniques, we achieve the outstanding OER performance of N, Ir-STO/Ti compared with the pristine STO/Ti. In addition, we further explore the influence of different plasma treatment time on the electrocatalytic performance of N, Ir-STO/Ti. It is found that suitable plasma treatment will improve the cacancy density of N, Ir-STO/Ti, which can improve the charge transport properties, resulting in superior OER performance. The N, Ir-STO/Ti electrode reveals excellent acidic OER activity with the lowest overpotential of 390 mV at 10 mA/cm^2 and the smallest Tafel slope of 140 mV/dec after 10-min NH_3 plasma treatment. With excessive plasma treatment, the redundant N atoms can easily occupy the oxygen vacancies, leading the vacancy concentration and mobility to decrease. The results reveal that a moderate plasma treatment can balance the generation of vacancies and N doping to obtain the best OER characteristics. Our studies make a new opportunity for designing electrocatalysts with significantly low noble metal content and providing a generic method to realize controllable doping of other perovskite catalysts via plasma treatment.

Acknowledgements

Project supported by the Priority Academic Program Development (PAPD) Program of Jiangsu Higher Education Institutions, Jiangsu Province, China and the National Natural Science Foundation of China (Grant No. 11675117).

References

[1] Cook T R, Dogutan D K, Reece S Y, Surendranath Y, Teets T S and Nocera D G 2010 *Chem. Rev.* **110** 6474
[2] Walter M G, Warren E L, McKone J R, Boettcher S W, Mi Q, Santori E A and Lewis N S 2010 *Chem. Rev.* **110** 6446
[3] Nathan S L 2006 *Proc. Natl. Acad. Sci. USA* **103** 15729
[4] Cao H, Chen M, Wu L, Hou G, Tang Y and Zheng G 2017 *Appl. Surf. Sci.* **428** 861
[5] Shan J, Guo C, Zhu Y, Chen S, Song L, Jaroniec M, Zheng Y and Qiao S Z 2019 *Chem* **5** 445
[6] Suen N T, Hung S F, Quan Q, Zhang N, Xu Y J and Chen H M 2017 *Chem. Soc. Rev.* **46** 337
[7] Lv H, Wang S, Li J, Shao C, Zhou W, Shen X, Xue M and Zhang C 2020 *Appl. Surf. Sci.* **514** 145943
[8] Reier T, Oezaslan M and Strasser P 2012 *ACS Cata.* **2** 1765
[9] Xu H, Shi Z X, Tong Y X and Li G R 2018 *Adv. Mater.* **30** 1705442
[10] Suntivich J, May K J, Gasteiger H A, Goodenough J B and Shao Horn Y 2011 *Science* **334** 1383
[11] Hardin W G, Mefford J T, Slanac D A, Patel B B, Wang X, Dai S, Zhao X, Ruoff R S, Johnston K P and Stevenson K J 2014 *Chem. Mater.* **26** 3368

[12] Liu Y, Li H J, Zhang Q, Li Y and Liu H T 2013 *Chin. Phys. B* **22** 057201

[13] Seitz Linsey C, Dickens Colin F, Nishio K, Hikita Y, Montoya J, Doyle A, Kirk C, Vojvodic A, Hwang Harold Y, Norskov Jens K and Jaramillo Thomas F 2016 *Science* **353** 1011

[14] Jin C, Cao X, Zhang L, Cong Z and Yang R 2013 *J. Power Sources* **241** 225

[15] Ji Q, Bi L, Zhang J, Cao H and Zhao X S 2020 *Int. J. Hydrogen Energy* **45** 12514

[16] Liang X, Shi L, Liu Y, Chen H, Si R, Yan W, Zhang Q, Li G D, Yang L and Zou X 2019 *Angew. Chem. Int. Ed. Engl.* **58** 7631

[17] Badreldin A, Abusrafa A E and Abdel-Wahab A 2020 *Emergent Mater.* **3** 567

[18] Mefford J T, Rong X, Abakumov A M, Hardin W G, Dai S, Kolpak A M, Johnston K P and Stevenson K J 2016 *Nat. Commun.* **7** 11053

[19] She S, Yu J, Tang W, Zhu Y, Chen Y, Sunarso J, Zhou W and Shao Z 2018 *ACS Appl. Mater. Interfaces* **10** 11715

[20] Sun B, He D, Wang H, Liu J, Ke Z, Cheng L and Xiao X 2021 *Chin. Phys. B* **30** 106102

[21] Liu X, Zhang L, Zheng Y, Guo Z, Zhu Y, Chen H, Li F, Liu P, Yu B, Wang X, Liu J, Chen Y and Liu M 2019 *Adv. Sci.* **6** 1801898

[22] Wang Z, Zhang Y, Neyts E C, Cao X, Zhang X, Jang B W L and Liu C 2018 *ACS Catal.* **8** 2093

[23] Lu Y, Ma A, Yu Y, Tan R, Liu C, Zhang P, Liu D and Gui J 2018 *ACS Sustain. Chem. Eng.* **7** 2906

[24] Ran J, Wang T, Zhang J, Liu Y, Xu C, Xi S and Gao D 2020 *Chem. Mater.* **32** 3439

[25] Xiong J, Zhong H, Li J, Zhang X, Shi J, Cai W, Qu K, Zhu C, Yang Z, Beckman S P and Cheng H 2019 *Appl. Catal. B: Environ.* **256** 117817

[26] Fuertes A 2012 *J. Mater. Chem.* **22** 3293

[27] Fuertes A 2015 *Mater. Horiz.* **2** 453

[28] Marlec F, Le Paven C, Le Gendre L, Benzerga R, Cheviré F, Tessier F, Gam F and Sharaiha A 2017 *Surf. Coat. Technol.* **324** 607

[29] Liu Y, Wang W, Xu X, Marcel Veder J P and Shao Z 2019 *J. Mater. Chem.* **7** 7280

[30] Zhang J, Zhang C, Li W, Guo Q, Gao H, You Y, Li Y, Cui Z, Jiang K C, Long H, Zhang D and Xin S 2018 *ACS Appl. Mater. Interfaces* **10** 5543

[31] Lee Y, Suntivich J, May K J, Perry E E and Shao H Y 2012 *J. Phys. Chem. Lett.* **3** 399

[32] Husein I F, Qin S, Zhou Y Z and Chan C 1997 *Nucl. Instrum. Method B* **121** 226

[33] Yu L, Bati A, Grace T, Batmunkh M and Shapter J 2019 *Adv. Energy Mater.* **9** 1901063

[34] Pansila P P, Kanomata K, Ahmmad B, Kubota S and Hirose F 2015 *IEICE T Electron.* **E98-C** 395

[35] Zhao J, Lu G, Wu Y, Zhang P, Yue J, Cheng Z, Zhang J and Kang X 2020 *Colloid. Surface A* **603** 125254

[36] Lan C K, Chuang S I, Bao Q, Liao Y T and Duh J G 2015 *J. Power Sources* **275** 660

[37] Tan X, Chen C, Jin K and Luo B 2011 *J. Alloys Compd.* **509** L311

[38] Shi X, Zhu H, Du J, Cao L, Wang X and Liang H P 2021 *Electrochimica Acta* **370** 137710

[39] Liu C M, Zu X T and Zhou W L 2007 *J. Phys. D: Appl. Phys.* **40** 7318

[40] Yang X, Zhao F, Yeh Y W, Selinsky R S, Chen Z, Yao N, Tully C G, Ju Y and Koel B E 2019 *Nat. Commun.* **10** 1543

[41] Chen Q, Ozkan A, Chattopadhyay B, Baert K, Poleunis C, Tromont A, Snyders R, Delcorte A, Terryn H and Delplancke Ogletree M P 2019 *Langmuir* **35** 7161

[42] Yu J, Wu X, Guan D, Hu Z, Weng S C, Sun H, Song Y, Ran R, Zhou W, Ni M and Shao Z 2020 *Chem. Mater.* **32** 4509

[43] Anantharaj S, Karthik P E and Kundu S 2015 *J. Mater. Chem. A* **3** 24463

[44] Guo Y, Wang T, Chen J, Zheng J, Li X and Ostrikov K 2018 *Adv. Energy Mater.* **8** 1800085

[45] Li Z, Lv L, Wang J, Ao X, Ruan Y, Zha D, Hong G, Wu Q, Lan Y, Wang C, Jiang J and Liu M 2018 *Nano Energy* **47** 199

[46] He T, Zeng X and Rong S 2020 *J. Mater. Chem. A* **8** 8383

[47] Zhang Y Q, Tao H B, Chen Z, Li M, Sun Y F, Hua B and Luo J L 2019 *J. Mater. Chem. A* **7** 26607

[48] Xinghua C, Lv M, Jin S, Wang H, Chen Y, Ma T, Cui K, Li J, Yong W, Liu Z, Guo Y, Liu Z and Li X 2020 *Catal. Sci. Technol.* **10** 4786

[49] Ma X, Zhou Y, Cao L, Wang K, Deng L, Fan R and Xin Y 2020 *Surf. Coat. Technol.* **396** 125961

[50] Liu Y, Liang X, Chen H, Gao R, Shi L, Yang L and Zou X 2021 *Chin. J. Catal.* **42** 1054

[51] Beknalkar S A, Teli A M, Harale N S, Patil D S, Pawar S A, Shin J C and Patil P S 2021 *Appl. Surf. Sci.* **546** 149102

[52] Xu L K and Scantlebury J D 2003 *Corros. Sci.* **45** 2729

[53] Hu M J, Meng M H, Zhang Q J and N C 2002 *Corros. Sci.* **44** 1655

[54] Zhou X, Zhou J, Huang G, Fan R, Ju S, Mi Z and Shen M 2018 *J. Mater. Chem. A* **6** 20297

[55] Lü G H, Chen H, Wang X Q, Pang H, Zhang G L, Zou B, Lee H J and Yang S Z 2010 *Chin. Phys. B* **19** 085202

[56] Shieh D T and Hwang B J 1993 *Electrochimica Acta* **38** 2239

[57] Da Silva L M, Fernandes K C, De Faria L A and Boodts J F C 2004 *Electrochimica Acta* **49** 4893

[58] Da Silva L M, De Faria L A and Boodts J F C 2002 *J. Electroanal. Chem.* **532** 141

[59] Liu C W, Xu J P, Liu L and Lu H H 2015 *Chin. Phys. B* **24** 127304

[60] Haynes W M 2014 *CRC handbook of chemistry and physics*, 95th edn. (New York: CRC Press) pp. 1603–1613